Article

Novel Treatment for Glioblastoma Delivered by a Radiation Responsive and Radiopaque Hydrogel

Mathilde Bouché,* Yuxi C. Dong, Saad Sheikh, Kimberly Taing, Deeksha Saxena, Jessica C. Hsu, Minna H. Chen, Ryan D. Salinas, Hongjun Song, Jason A. Burdick, Jay Dorsey, and David P. Cormode*
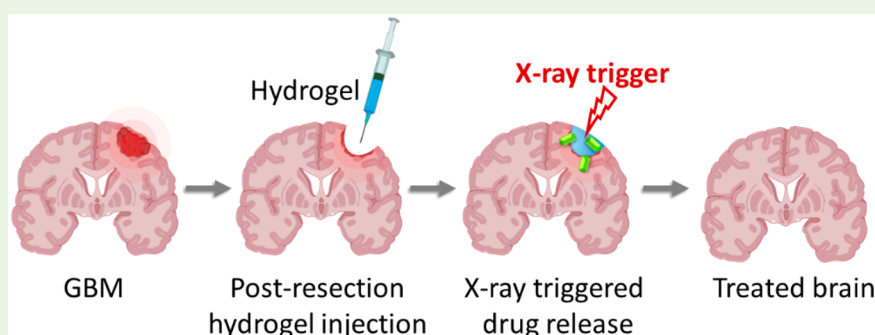
Read Online

ACCESS | Metrics & More | Article Recommendations | Supporting Information

ABSTRACT: Successful treatment of glioblastoma (GBM) is hampered by primary tumor recurrence after surgical resection and poor prognosis, despite adjuvant radiotherapy and chemotherapy. In search of improved outcomes for this disease, quisinostat appeared as a lead compound in drug screening. A delivery system was devised for this drug and to exploit current clinical methodology: an injectable hydrogel, loaded with both the quisinostat drug and radiopaque gold nanoparticles (AuNP) as contrast agent, that can release these payloads as a response to radiation. This hydrogel grants high local drug concentrations, overcoming issues with current standards of care. Significant hydrogel degradation and quisinostat release were observed due to the radiation trigger, providing high in vitro anticancer activity. In vivo, the combination of radiotherapy and the radiation-induced delivery of quisinostat from the hydrogel, successfully inhibited tumor growth in a mice model bearing xenografted human GBM tumors with a total response rate of 67%. Long-term tolerability was observed after intratumoral injection of the quisinostat loaded hydrogel. The AuNP payload enabled precise image-guided radiation delivery and the monitoring of hydrogel degradation using computed tomography (CT). These exciting results highlight this hydrogel as a versatile imageable drug delivery platform that can be activated simultaneously to radiation therapy and potentially offers improved treatment for GBM.

KEYWORDS: stimuli-responsive materials, hydrogels, drug delivery, glioblastoma, computed tomography

1. INTRODUCTION

Patients suffering glioblastoma (GBM), a common and aggressive form of primary brain tumor,[1,2] are still facing a poor prognosis with median survival below 15 months[3] despite surgery and adjuvant chemo- and radiation therapy.[4,5] This arises from glioblastoma stem cell (GSC) populations[6,7] that survive chemoradiotherapy[8,9] and induce significant tumor recurrence and disease relapse.[10−12] Furthermore, both the limitations in the radiotherapy dose deliverable to the GBM area to prevent brain damages, and the challenges in delivering high drug doses past the blood brain barrier (BBB)[13−15] emphasize the need for the development of local delivery systems for therapeutics. Gliadel, a biodegradable wafer, highlighted the potential of local treatments of GBM by implantation of a drug delivery platform in the resection cavity,[16] offering reduced toxicity compared to systemic injections.[17] However, this system hardly allows the admin-

istration of the therapeutic dose, which resulted in limited improvement of the patient survival by 2 months.[18,19]

Seeking for a more effective treatment of GBM, we performed a high throughput screen for more effective drugs that display concomitant integrated stress response-dependent death receptor expression.[20] Quisinostat (QS) was identified as a lead compound based on its significant anti-GBM activity and elevated expression of death receptors for a dual action toward GSC. We found it to be highly effective against GBM, and developed a delivery system for this drug to limit systemic

adverse effects at the therapeutic dose and enhance delivery directly to the GBM area. While other hydrogels are bioerodible[21] or stimuli-responsive,[21−25] their therapeutic effect could be hampered by the potentially deep location of GBM and thereby lack of access of drug release triggers, we developed an X-ray radiation responsive hydrogel to permit a limitless depth penetration trigger of drug delivery. Poly di(carboxylatophenoxy)phosphazene (PCPP) has an excellent in vivo safety profile[26−28] and can be physically cross-linked via electrostatic interactions with cations such as polyamines.[29−34] Therefore, herein PCPP was physically cross-linked with the radiation responsive selenocystamine (pK_a = 8.9) to form an injectable hydrogel termed Se-PCPP. Quisinostat was loaded in the hydrogel with a contrast agent to permit in vivo tracking by computed tomography (CT), that is, radiopaque sub-5-nm gold nanoparticles (AuNP) that have strong contrast attenuation.[33,34] Loading a CT active contrast agent in the hydrogel is of importance for precise image-guided radiation delivery to GBM that are deeply lying tumors and monitoring over time. Moreover, CT has a limitless signal depth and is quantitative, low-cost, and widely available in hospitals, making it an attractive imaging modality for GBM. Moreover, radiotherapy systems typically have integrated CT systems, which are used to scan the patient prior to each administration of radiation; therefore, this approach fits with clinical procedures.

Our findings suggest that our quisinostat and AuNP-loaded hydrogel formulation can successfully be administered intratumorally by syringe and visualized by CT. We also emphasize the activation of this formulation by a radiation trigger to release on-demand quisinostat and treat glioblastoma with a total response rate of 67% and showing no signs of long-term relapse.

2. EXPERIMENTAL SECTION

2.1. Materials. Gold(III) chloride trihydrate, sodium borohydride, poly(bis(4-carboxyphenoxy)phosphazene) disodium salt (PCPP, 1 MDa), L-glutathione reduced (GSH), selenocystamine dihydrochloride, hexamethylenediamine, doxorubicin and albumin-fluorescein conjugate were purchased from Sigma-Aldrich (St. Louis, MO). Quisinostat dihydrochloride was purchased from Selleckchem (Houston, TX). HepG2, U251, Renca, and SVEC4-10 cell lines were purchased from ATCC (Manassas, VA). LIVE/DEAD assay kits were purchased from Life Technologies Invitrogen (Grand Island, NY). Cells were cultured in Dubecco's Modified Eagle Medium supplemented with 10% fetal bovine serum and 1% penicillin (10000 units/mL) from Life Technologies Invitrogen (Grand Island, NY). Athymic nude mice were obtained from Charles River Laboratories (stock no. 490).

2.2. Cell-Based High-Throughput Death Receptor Screen. High-throughput screening (HTS) was performed by the HTS core at the University of Pennsylvania. U251 DR5-Luc cells were plated at 2.0 × 10³ cells/well across ten 384-well plates. Plates were then incubated in a humidified environment at 37 °C and 5% CO_2 for 24 h. Compounds from the Selleckchem Bioactive Compound Library I was added to each well at 100 nM (approximately 3200 compounds). Tunicamycin (100 nM) and DMSO (0.1% v/v) served as positive and negative plate controls. Brite-Lite (PerkinElmer, Waltham, MA) reagent was added all plates 24 h following the addition of compound, and plates were assayed on Envision Xcite (PerkinElmer) plate reader. The mean (μ) and standard deviation (σ) for each plate was used to transform total flux for each compound (x_i) into z-scores using the formula $z = (x_i − \mu/\sigma)$. Calculation of z-prime for this screening assay utilized tunicamycin and DMSO as a positive and negative controls, respectively. Positive hits were identified as compounds that produced z-prime values greater than tunicamycin. Reporter activity was

validated following compound incubation and bioluminescence imaging on the IVIS spectrum (PerkinElmer).

2.3. Western Blot Analysis. Western blot analysis was performed as previously described.[20]

2.4. Compound Dilution Studies and Cell Viability. Cells were plated at density of 7.5−1.0 × 10⁴ cells/well in 96 well plates using their respective media. Plates were then incubated in a humidified environment at 37 °C and 5% CO_2 for 24 h. An 11-point dilution series of positive hits from our HTS screen was added to each plate. Cells treated with 0.1% DMSO served as a vehicle control. Plates were incubated with compound for 72 h at 37 °C and 5% CO_2, followed by addition of Cell Titer Glo (Promega). Bioluminescent readings were obtained using a Synergy HT luminometer (BioTek, Winooski, VT). Raw bioluminescent values were normalized to their vehicle treated controls, and then fit to a modified Hill Equation using OriginPro 8 (OriginLab, Northampton, MA) in order to calculate IC_{50} values. All dilution series experiments were performed as biological triplicates.

2.5. Sphere Formation Assay. T4213 and NS039 cells were plated at 2000 cells/well in 6-well plates in the presence of 0.1% DMSO or 1.0 μM Quisinostat in biological triplicate for 12 days. On day 12, individual wells were imaged on a Lionheart Fx microscope at 4× magnification following addition of NucBlue (Hoechst 33342, Invitrogen). Circular blue objects greater than 50 μm in diameter and less than 750 μM were counted as neurospheres. Differences in sphere formation between cells and treatments were assessed using a one-way ANOVA followed by posthoc Tukey's test in GraphPad Prism 8. P-values less than 0.05 were considered significant.

2.6. Primary Brain Tumor Specimens. As previously described,[20] the use of primary tumor tissue was coordinated by the University of Pennsylvania Tumor Tissue/Biospecimen Bank following ethical and technical guidelines on the use of human samples for biomedical research purposes. Patient GBM tissues were collected at the Hospital of the University of Pennsylvania after informed patient consent under a protocol approved by the University of Pennsylvania's Institutional Review Board. All patient samples were deidentified before processing. Mutational status of clinical glioblastoma tissue was made available from a routinely performed clinical sequencing panel.

2.7. Brain Tumor Organoids, Compound Incubation, and Viability. Glioblastoma organoids (GBOs) were generated from primary brain tumor as previously described.[20] Briefly, primary brain tumor specimens were minced into approximately 1 mm³ pieces following clinical confirmation of pathologic diagnosis and incubated in GBO medium containing 50% DMEM:F12 (Thermo Fisher Scientific), 50% Neurobasal (Thermo Fisher Scientific), 1× GlutaMax (Thermo Fisher Scientific), 1× NEAAs (Thermo Fisher Scientific), 1× PenStrep (Thermo Fisher Scientific), 1× N2 supplement (Thermo Fisher Scientific), 1× B27 w/o vitamin A supplement (Thermo Fisher Scientific), 1× 2-mercaptoethanol (Thermo Fisher Scientific), and 2.5 μg/mL human insulin (Sigma) per well and placed on an orbital shaker rotating at 120 rpm within a 37 °C, 5% CO_2, and 90% humidity sterile incubator.

Organoids would generally form 2−4 weeks following initial culturing. Organoids were then incubated in media containing either vehicle (0.1% DMSO) or 1.0 μM quisinostat with media changes every 2 days for 7 days total. Post-treatment images were taken on brightfield microscope and samples were subsequently fixed in 4% paraformaldehyde × 30 min for immunofluorescence analysis.

2.8. Immunofluorescence. As previously described, serial tissue sections (20 μm) were sliced using a cryostat (Leica, CM3050S), and melted onto charged slides (Thermo Fisher Scientific). Slides were dried at room temperature and stored at −20 °C until ready for immunohistology. For immunofluorescence staining, the tissue sections were outlined with a hydrophobic pen (Vector Laboratories) and washed with TBS containing 0.1% Tween-20 (v/v). Nonspecific binding was blocked using a solution containing 10% donkey serum (v/v), 0.5% Triton X-100 (v/v), 1% BSA (w/v), 0.1% gelatin (w/v), and 22.52 mg/mL glycine in tris-buffered saline-Tween (TBST) for 1 h at room temperature. The tissue sections were incubated with

primary antibodies against Ki67 (BD Biosciences catalog no. 550609) and Cleaved-Caspase 3 (Cell Signaling Technology catalog no. 9661) diluted in TBST with 5% donkey serum (v/v) and 0.1% Triton X-100 (v/v) overnight at 4 °C. After they were washed in TBST, the tissue sections were incubated with secondary antibodies (Alexa Fluor 555 and 647, respectively) diluted in TBST with 5% donkey serum (v/v) and 0.1% Triton X-100 (v/v) for 1.5 h at room temperature. After washing with TBST, sections were incubated with TrueBlack reagent (Biotium) diluted 1:20 in 70% ethanol for 1 min to block autofluorescence because of lipofuscin and blood components. After washing with DPBS, slides were mounted in mounting solution (Vector Laboratories), coverslipped, and sealed with nail polish.

GBOs were imaged on a Zeiss LSM 710 confocal microscope (Zeiss) using a 20X objective with Zen 2 software (Zeiss). Images were quantified and analyzed using ImageJ software. Graphical and statistical analysis was performed using GraphPad Prism 8 software.

2.9. Orthotopic Tumor Implantation and Treatment with Quisinostat. All animal work was approved by the Institute for Animal Care and Use Committee at the University of Pennsylvania (no. 805893). T4213 cells were stably modified using a lentiviral vector containing green fluorescent protein (GFP) and Luciferase (Biosettia, San Diego, CA). Cells were resuspended in serum free media, and then, 3.0×10^5 cells were stereotactically injected into the right striatum of five-week female athymic nude mice (Charles River Laboratories). Tumor bioluminescence was quantified on the IVIS spectrum (PerkinElmer) following intraperitoneal administration of D-Luciferin (Goldbio, St Louis MO) 2 days, following cell implantation. In a separate experiment, mice underwent serial bioluminescence imaging following orthotopic T4213 implantation. Mice were assigned to different treatment groups such that the total flux (photons/s) was equivalent between groups (6.4×10^6 photons/s). Treatment was initiated immediately following bioluminescent imaging and consisted of once daily intraperitoneal administration of 2-hydroxypropyl-β-cyclodextrin (vehicle, Cayman Chemical, Ann Arbor MI) or 10 mg kg^{-1} quisinostat (Cayman Chemical) for a total of eight doses. Mice were given a 72 h break between treatments if they demonstrated weight loss, dehydration, or lethargy (Figure S4). Bioluminescent imaging was repeated 72 h after the last treatment was administered. Mice were weighed two to three times per week throughout all experiments until they met criteria for humane euthanasia (loss of 20% of body weight, neurologic deficits). Following humane euthanasia, brains were carefully removed and stored in 10% Neutral Buffered Formalin at 4 °C. Selected brains were sent to the Cancer Histology Core at the University of Pennsylvania for paraffin embedding followed by hematoxylin and eosin staining. Serial bioluminescence was assessed using a one-way repeated measures ANOVA followed by a posthoc Tukey test. Post-treatment total flux was background corrected, and the percent change in total flux was analyzed using a Mann−Whitney U test. Both analyses were performed in GraphPad Prism 8, and p-values less than 0.05 were considered significant.

2.10. Gold Nanoparticle Synthesis. The gold nanocrystals were synthesized via a modification of the method of Turkevich by reduction of gold(III) chloride with sodium borohydride and subsequent surface modification with a stabilizing ligand.[29] $AuCl_3 \cdot 6H_2O$ was dissolved in deionized (DI) H_2O (8 mg mL^{-1}, 100 mL) under stirring. A freshly prepared solution of $NaBH_4$ (5 mg mL^{-1}, 2 mL DI H_2O) was dropped to the gold chloride solution and allowed to stir at room temperature for 20 min. Then, a solution of the capping glutathione (GSH, 5.2 mg mL^{-1}, 1 mL DI H_2O) was added to the mixture, which was further transferred to 50 mL plastic tubes and incubated at 4 °C overnight. Concentration and purification of AuNP were performed using molecular weight cut off tubes (10 kDa MWCO tubes), centrifuged at 4000 rpm, rinsed twice with DI H_2O to afford the purified AuNP. Inductively coupled plasma optical emission spectroscopy (ICP-OES) was performed on a Spectro Genesis ICP to determine the final gold concentration of the stock solution.

2.11. Se-PCPP Hydrogel Formulation. *2.11.1. Se-PCPP Hydrogel.* A mixture of 1 mL of PCPP (4 mg mL^{-1}, PBS) and 10.3 mg Na_2HPO_4 were mixed together and pH was adjusted to 7.4 by

addition of HCl (1 M). Next, selenocystamine dihydrochloride (0.48 mmol, 110 mg.mL^{-1}, PBS) was added to the mixture and vortexed for 30 s. The mixture was dropped into 10 mL of a $CaCl_2$ (8.8%, DI H_2O) and left to react under vigorous stirring for 20 min at room temperature. Finally, the solution was transferred to conical tubes and centrifuged at 2 k rpm for 8 min. The supernatant was discarded, and the pellet was resuspended in DI water. After repeating this process three times, the Se-PCPP solution was resuspended in DI water, vortexed at 14 k rpm and stored at 4 °C. The final concentration of AuNP in the sample was determined using inductively coupled plasma spectrometry (ICP-OES) performed on a Spectro Genesis ICP.

2.11.2. Cargo-Loaded Se-PCPP Hydrogel. For the cargo-loaded Se-PCPP hydrogel, the PCPP (1 mg, 4 mg mL^{-1}, PBS) solution was mixed with the cargo (370 μg of doxorubicin, 46 μg of albumin bovine serum−fluorescein thioisocyanate conjugate (FITC-BSA), or 405 μg of quisinostat), AuNP (10 mg), and 10.3 mg of Na_2HPO_4. The total volume was completed to 2 mL with PBS; the pH was adjusted to 7.4 by addition of HCl (1 M), and the mixture was incubated for 10 min before cross-linking with selenocystamine dihydrochloride as described above. The final drug concentration in the sample were determined using UV−vis spectroscopy by determining the encapsulation efficiency (EE), calculated as EE = [stock drug] − ([nonloaded drug]/[stock drug]); and the drug content, calculated as drug content = $m_{\text{stockdrug}} \times$ EE.

2.11.3. C-PCPP Hydrogel. The non-X-ray sensitive hydrogel was synthesized following the same procedure as described above, using a solution of hexamethylenediamine (0.48 mmol, 65 mgmL^{-1}) for cross-linking and hydrogel formation, in place of selenocystamine.

2.12. UV−vis Spectroscopy. The UV−vis absorption spectrum of GSH-AuNP and Se-PCPP hydrogels were recorded on a UV/visible spectrophotometer (Thermo Fisher Scientific, USA) after dilution in DI water.

2.13. Transmission Electron Microscopy (TEM). For air-dried samples, the samples were deposited onto a copper grid and allowed to dry for a minimum of 24 h prior image acquisition. For embedded samples, hydrogels were fixed with 2% paraformaldehyde and 2.5% glutaraldehyde, embedded, cut into sections of 60 nm thickness and mounted onto copper grids. TEM images were acquired at 80 keV using a JEM 1010 microscope (JEOL, Tokyo, Japan) with an AMT NanoSprint500 5 Megapixel (AMT, Woburn (MA), USA).

2.14. Scanning Electron Microscopy (SEM). Samples were freeze-dried shortly before the acquisition of SEM images using a Quanta 250 (FEI, Hillsboro, OR) at near atmospheric pressure, with a gaseous secondary electron detector.

2.15. Fourier Transform Infrared (FT-IR). Five microliter samples were ground with 100 mg of potassium bromide (KBr) and pressed into pellet; the transmission spectrum of Se-PCPP hydrogel was collected on a JASCO FT/IR-480 PLUS.

2.16. Inductively Coupled Plasma Optical Emission Spectroscopy (ICP-OES). Gold and phosphorus concentrations in the hydrogels were determined using ICP-OES (Spectro Genesis ICP). The samples were prepared by dissolving 10 μL of sample stock solution in 1 mL of aqua regia and making the final volume up to 6 mL with DI water.

2.17. Vial Inversion. The gel characteristics of the Se-PCPP hydrogel were initially assessed by performing the vial inversion method. Briefly, the samples were transferred to vials and allowed to stand reversed for 1 h. All mixtures that remained unchanged and without dropping were considered as having the characteristics of a gel.

2.18. Rheology. The hydrogels were sonicated for 30 min in an ultrasound bath before loading onto the rheometer. The rheometer experiments were conducted using a parallel plate geometry, a gap size of 100 μm, and the following measurements were carried out at 25 °C: frequency sweep (0.01−100 Hz, 0.2% strain), time sweep (0.2% strain, 10 Hz), strain sweep (0.01−500% strain, 10 Hz), continuous flow (shear rates from 0 to 50 s^{-1} over 2 min 30 s), and cyclic strain (low = 0.2% strain, high = 500% strain, 10 Hz).

2.19. Injection Force. The hydrogels were sonicated for 30 min in an ultrasound bath before loading 50 μL of the sample into a 1 mL

syringe assembled with a 25-gauge needle. The syringe was placed into an Instron 5848 microtester (Norwood, MA) and the load cell was placed in close vicinity to the plunger before initiating the experiment with a flow rate of 2 mL/h, while recording the maximum force applied during hydrogel extrusion over time. Testing was carried out in air and repeated 6 times.

2.20. X-ray Irradiation. The radiation dose delivered to the sample is quantified in gray (Gy) with the relation of $1 \text{ Gy} = 1 \text{ J kg}^{-1}$. The X-ray irradiation was performed on an X-RAD 320ix irradiator (PXi, North Branford, CT) operated at 320 kV, 12.5 mA, focal spot of 8 mm^2 and with an aluminum filter of 2 mm delivering a dosage rate of 2.65 Gy/min. In brief, the Se-PCPP hydrogel was sampled into 1 mL tube and placed in the irradiator chamber for the desired time depending onto the X-ray dose to be delivered.

2.21. Hydrogels Degradation and Cargo Release Experiments. Se-PCPP hydrogel ([Au] = 0.2 mg·mL^{-1}, [QS] = 12.5 ng·mL^{-1}) was suspended into 1 mL of freshly prepared PBS/10% FBS in microcentrifuge tubes and centrifuged at 4 krpm for 8 min. Samples were irradiated with the desired X-ray dose and incubated at 37 °C for the overall experiment time. At the desired time point, samples were vortexed, centrifuged at 4 k rpm for 8 min and the supernatant was gently collected for quantification of the released cargo by ICP-OES or UV−vis spectroscopy. One milliliter of freshly prepared incubation medium was rapidly added to each sample, all were incubated at 37 °C until the next time point.

2.22. Cell Culture. HepG2, Renca, SVEC4-10, U251, and NS039 cell lines were cultured according to the supplier's instructions, and all experiments were performed in triplicate.

LIVE/DEAD assay was performed to assess the biocompatibility of Se-PCPP hydrogel. Cells were plated in 6 wells plate at a density of 100 k cells per well. After 24 h incubation, the cells were treated with Se-PCPP hydrogel at concentrations of 0, 0.125, 0.25, and 0.5 mg/mL. After incubation at 37 °C, 5% CO$_2$ for 24 h, the cells were washed twice with DBPS and incubated for another 20 min with 400 μL of LIVE/DEAD cocktail (0.025% stock Calcein and 0.1% stock ethidium-1 homodimer in DPBS). Three images of four different areas of each well were acquired (excitation/emission filter pairs, 495/515 nm, and 528/617 nm, for Calcein or Ethidium Homodimer-1, respectively). Cell counts for each dye in each image was performed using a custom MATLAB code, and the ratio of dead to living cells normalized to control was calculated as the viability measurement.

2.23. Anti-GBM Effect of the Hydrogel Administration in Combination with Radiotherapy. *2.23.1. Effect of X-ray (XR) Trigger on the Drug Release.* An MTS assay was performed to assess the cytotoxicity of the drug released from the hydrogel on GBM cells U251 and NS039. Cells were plated in a 96-well plate at a density of 5000 cells per well and incubated at 37 °C, 5% CO$_2$ for 24 h. In the meantime, the drug-loaded hydrogel (1 mg of PCPP, 405 μg of QS) was incubated in cell medium, at 37 °C, for 24 h post X-ray irradiation (0 Gy for drug elution or 60 Gy for X-ray triggered drug release). Then, the drug containing supernatants were used to treat GBM cells for 48 h at 37 °C, 5% CO$_2$. Cells were finally rinsed with PBS once and incubated with MTS solution (20 μL stock solution in 100 μL cell medium) 30 min prior absorbance measurement at 490 nm with a plate reader (Synergy H1, BioTek, VT).

2.23.2. Effect of XR Trigger on the Drug Release Combined with Radiation Therapy (RT) Administration to the Cells. The Se-PCPP and C-PCPP hydrogels were prepared as detailed in section 2.11 to load 310 μg of QS per 1 mg of PCPP and 5 mg of AuNP, diluted with sterile DMEM cell culture medium (supplemented with 10 mL 50× B27, 12.5 mL 100 mM pyruvate, 10% PBS, and 1% PS) to [Au] = 0.2 mg mL^{-1}, and irradiated with 0 or 60 Gy (mock and treatment dose respectively) before 24 h incubation at 37 °C. The NS039 cells were plated as detailed above, treated with the drug containing supernatants from the irradiated hydrogels, then irradiated with 8 Gy radiotherapy and further incubated for 48 h at 37 °C in 5% CO$_2$ atmosphere. After 48 h, the MTS assay was performed to assess the cytotoxicity of the drug released from the hydrogels on NS039 as per the supplier's guidelines. The absorbance was measured at 490 nm with a plate reader.

2.24. Computed Tomography (CT) Phantom Imaging. Samples of different Au/P ratio were prepared into 250 μL vial tubes and secured in a plastic rack. A MiLabs μ-CT was operated at a tube voltage of 55 kV with tube current of 190 μA and exposure of 75 ms to acquire the CT images. Slices of 100 μm thickness with an increment of 0.1 mm were reconstructed using the algorithm provided by the manufacturer. Image analysis was performed using OsiriX (v.3.7.1 64-bit software). A circular ROI was drawn on the coronal view of each tube and the mean attenuation value for the ROI of five slices per tube was recorded and normalized to the value of the nonloaded Se-PCPP hydrogel. The reported attenuation value for each concentration correspond to the average of three samples of that same concentration.

2.25. In Vivo Rodent Model of Xenografted GBM. All the mouse work was performed under an approved protocol (Institutional Animal Care and Use Committee, IACUC) at the University of Pennsylvania (No. 805893). NS039 cells were resuspended in PBS, and then, 1.0×10^6 cells were subcutaneously implanted on the right flank of athymic nude mice and allowed to grow to a volume of approximately 100 mm^3. Daily monitoring of the mice was performed, ensuring the cage cleanliness, adequate water and food as well as good mouse activity. Both tumor growth and mice weight were measured every other day. Tumor length and width were measured with an electronic caliper and the volume was determined as $V = (\text{length} \times \text{width}^2)/2$. Tumors were allowed to grow up to $V = 15 \text{ cm}^3$ as per IACUC standards, after which animals were sacrificed.

2.26. Intratumoral Injection. All mice were first anesthetized with isoflurane, then were administered an intratumoral injection of 50 μL of treatment as follows: group 1, untreated ($n = 5$); group 2, radiotherapy ($n = 6$); group 3, radiotherapy + hydrogel ($n = 6$); group 4, hydrogel + drug ($n = 6$); group 5, hydrogel + drug + radiotherapy ($n = 6$). Hydrogel concentration [Au] = 8 mg mL^{-1}. Drug concentration [QS] = 648 ng mL^{-1}. Radiotherapy dose XR = 10 Gy.

2.27. In Vivo CT Imaging and Radiotherapy. *2.27.1. In Vivo CT.* The mice were first anesthetized with isoflurane; then, the CT images were acquired on a SARRP (Gulmay Medical, Inc., Camberley, United Kingdom) cone-beam CT at 50 kVp, 0.5 mA, and 1440 projections were used to reconstruct the images using the algorithm provided by the manufacturer. Image analysis was performed using OsiriX (v.3.7.1 64-bit software). Region of interest (ROI) was measured using the ROI segmentation tool to delineate the hydrogel from surrounding tissues; the hydrogel was reconstructed in 3D volume, and ROI was measured as the ROI values normalized to the muscle, and summed across the hydrogel.

2.27.2. In Vivo Radiotherapy. Twenty-four hours postinjection of the hydrogel, the mice (groups 3, 4, and 5) were anesthetized with isoflurane and were administered an X-ray dose of 10 Gy focused onto the tumor, delivered with a SARRP (Gulmay Medical, Inc., Camberley, United Kingdom), through a 17 mm diameter collimator mounted with a 0.15 mm copper filter and at a distance of 35 cm separating the mouse to the source.

2.28. Survival Analysis of Xenografted Mice. The survival time until the mice reached the maximum tumor growth as per IACUC standards, was calculated from the date of cell implantation (day −20). Mice were sacrificed if showing signs of distress, including excessive weight loss (>20%), lethargy, tumor metastasis, in accordance with IACUC standards.

2.29. Organs Harvesting and Ex Vivo Investigations. The mice were first euthanized with CO$_2$, followed by cervical dislocation as per IACUC recommendations. Then the abdominal cavity was opened to perform left ventricle perfusion with 20 mL of cold PBS, and finally, dissection was performed to harvest the major organs (heart, lungs, liver, spleen, kidneys) and the tumor. All organs were washed with cold PBS, transferred to 10% buffered formalin solution, cut to small pieces keeping aside one sample for histopathological investigation and the remaining for gold quantification.

2.29.1. Ex Vivo Biodistribution of Gold. Organ pieces were digested by 1 mL of HNO$_3$ for 17 h at 75 °C, and one more hour at 75 °C with 250 μL of HCl. All solutions were diluted with DI H$_2$O to
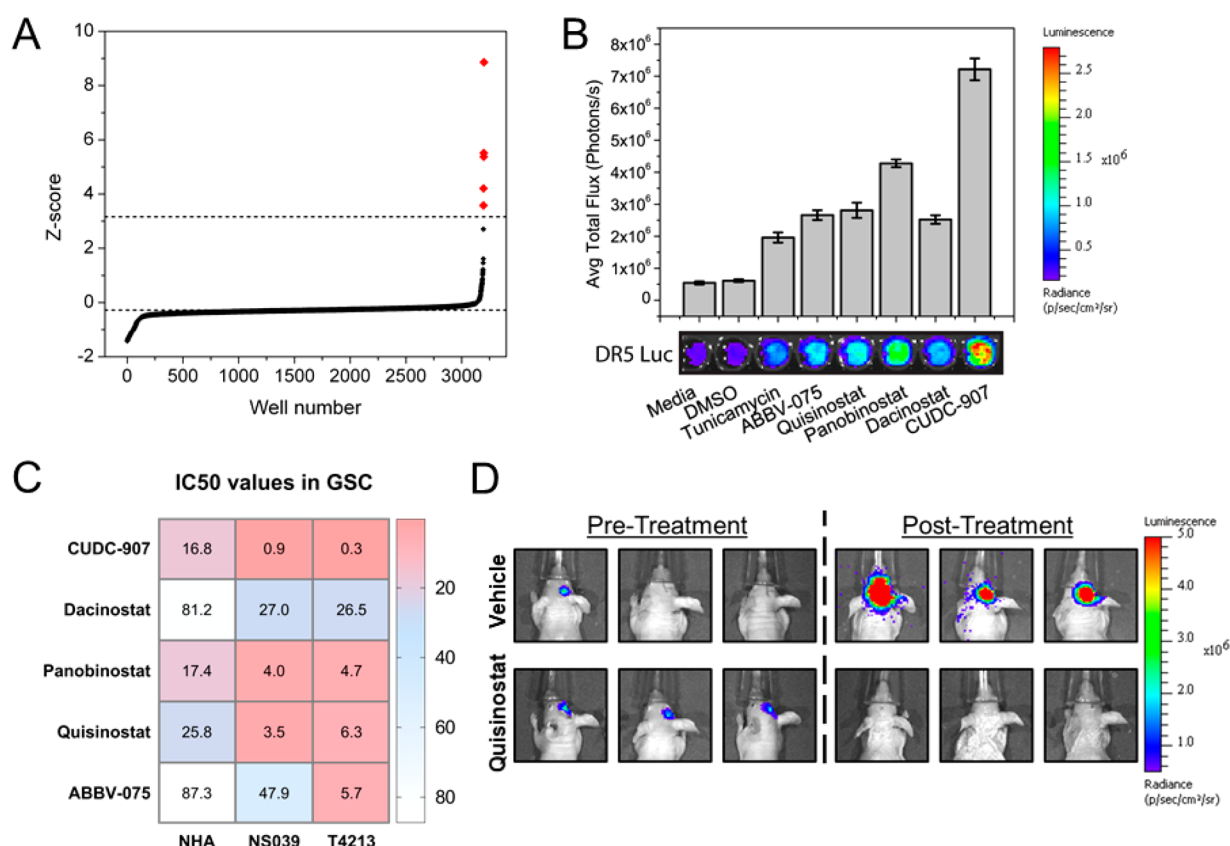
Figure 1. Identification of antiglioblastoma drug candidates. (A) Results of a high throughput screen of over 3000 compounds using a bioluminescence-based assay quantifying death receptor expression levels, and converting total flux into z-scores and (B) quantification of the levels of death receptor expression induced by the five lead compounds (100 nm) via bioluminescence imaging. (C) IC_{50} values found for the five lead compounds against normal human astrocytes (NHA) and glioblastoma cell lines (NS039 and T4213) after 72 h of treatment and (D) validation of the in vivo antiglioblastoma activity of quisinostat by bioluminescence imaging.

a final volume of 6 mL, centrifuged (1 krpm, 10 min), and filtered prior gold quantification using ICP-OES.

2.29.2. Histopathological Tissue Analysis. The organ slice was fixed in 10% buffered formalin solution and kept at −4 °C until further processing with sequential dehydration in increasing concentrations of ethanol and storage at −20 °C. Finally, organ slices were embedded in paraffin, sectioned, stained with hematoxylin and eosin dyes (H&E), and analyzed with a slide scanner Aperio CS-O (Leica Biosystems).

2.30. Statistical Analysis. Each experiment was performed at least in three replicates, unless stated otherwise. A one-way ANOVA test was performed on the Excel software for statistical analysis, and the data were considered nonstatistically significant for $p > 0.05$.

3. RESULTS

3.1. Cell-Based Death Receptor Uncovers Epigenetic Agents. Our cell-based death receptor assay used bioluminescence to identify the potent drugs capable to induce an integrated stress response-dependent death receptor expression among over three thousand compounds that were screened.[20] Converting the total bioluminescence flux into z-scores using the formula $z = (x_i - \mu)/\sigma$, and comparing to both tunicamycin and DMSO as positive and negative controls, respectively, we uncovered five promising hits, that is, quisinostat, panobinostat, CUDC-907, ABBV-075, and dacinostat (Figure 1A and B).[20] Quisinostat, panobinostat, and CUDC-90, which are epigenetic drugs, led to single digit nanomolar IC_{50} values in two glioblastoma cell lines, that is, NS039 and T4213 (Figure 1C). Overall, quisinostat was

selected as a promising hit over CUDC-907 and panobinostat because of its low toxicity on normal human astrocytes (NHA), high efficacy in both NS039 and T4213, and its ability to generate C/EBP homologous protein (CHOP) dependent death receptor 5 (DR5) expression at nanomolar concentrations (Figure S1A and B) and motivated its use to pursue investigations herein on its local delivery from our hydrogel.

3.2. GBM Stem Cell and Organoid Viability Is Reduced Following Quisinostat Treatment. Incubation of T4213 and NS039 cells with quisinostat significantly reduced neurosphere formation at 12 days (Figure S2A, $p <$ 0.05) while intact neurospheres are observed in controls by Hoechst staining (Figure S2B).[35] Moreover, quisinostat incubation with five distinct lines of patient derived glioblastoma organoids (GBOs) resulted in a shrunken and fragmented cell morphology accompanied by a loss of sphere formation and integrity, while caspase and antigen Ki67 staining further support the therapeutic efficacy of this drug (Figure S3).

3.3. GSC Viability Is Reduced Following in Vivo Treatment with Quisinostat. Orthotopic implantation of luciferase labeled T4213 cells produced a tumor that mimics features of aggressive GBM (Figure S4A) and mice treated once daily with 10 mg/kg quisinostat demonstrated a noticeable decrease in tumor bioluminescence suggesting tumor volume decrease (Figures 1D and S4B and C). On the other hand, tumor bioluminescence either remained stable or increased in vehicle treated mice suggesting tumor growth
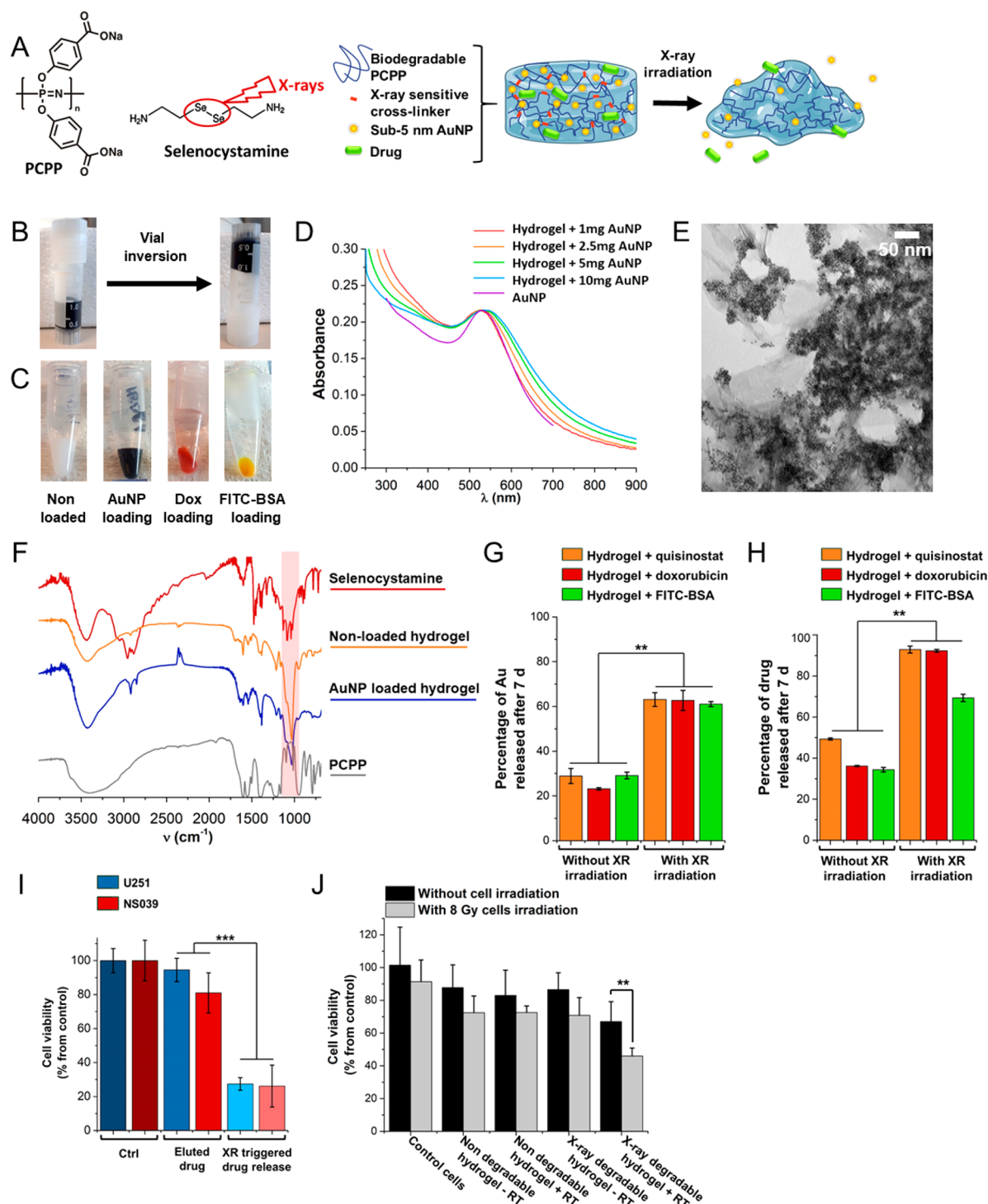
Figure 2. (A) Chemical structures and schematic representation of the radiation triggered release of drug and small AuNP payloads from Se-PCPP hydrogel. (B) Photograph of the Se-PCPP hydrogel loaded with 405 μg quisinostat and 10 mg of AuNP per 1 mg of PCPP, before and after the vial inversion test. (C) Photograph of the Se-PCPP hydrogel nonloaded, or loaded with 10 mg of AuNP, 370 μg of doxorubicin, or 46 μg of FITC-BSA per 1 mg of PCPP (left to right) with some excess water on top of the hydrogel for storage purposes. (D) UV−vis spectra of Se-PCPP hydrogel loaded with increasing amounts of AuNP (from 1 to 10 mg AuNP per 1 mg PCPP) compared to free AuNP and acquired at constant gold concentration. (E) Representative TEM of the Se-PCPP hydrogel in dry state loaded with 5 mg AuNP per 1 mg PCPP. Scale bar = 50 nm. (F) FT-IR spectra of the nonloaded (*orange*) and AuNP loaded (*blue*) Se-PCPP hydrogel and comparison to free selenocystamine (*red*) and free PCPP (*gray*). Comparison of the release (after 7 days incubation) of (G) AuNP and (H) drug between mock irradiation (*left*) and 60 Gy radiation triggered degradation (*right*) from the Se-PCPP hydrogel containing quisinostat (*orange*), doxorubicin (*red*), or FITC-BSA (*green*). (I) Viability of U251 (*blue*) and NS039 (*red*) cells after incubation with cell medium treated with either the eluted drug from the non-irradiated Se-PCPP loaded with quisinostat, or the radiation released drug from the Se-PCPP loaded with quisinostat and irradiated with 60 Gy. (J) Viability of NS039 cells without (*black*) or with 8 Gy irradiation, (*gray*) and treated with either vehicle, the nondegradable hydrogel loaded with quisinostat and our X-ray degradable hydrogel loaded with quisinostat. ** and *** indicate a difference at $p < 0.01$ or 0.001, respectively.

(Figures 1D and S4D). Although these findings highlighted the therapeutic potential of quisinostat to reduce the viability of GBM stem cell populations, systemic administration of quisinostat resulted in reduction of mouse body weight (Figure S4E) and diminished mouse activity and motivated the development of a localized delivery system devised to enhance the delivery of this drug straight to the GBM area.

3.4. Synthesis, Characterization, and Contrast Enhancement in CT of the Se-PCPP Hydrogel. Our hydrogel formulation, termed Se-PCPP (Figure 2A), consists of cross-linking PCPP polymer with selenocystamine and can load large amounts of radiopaque AuNP (5 mg AuNP per 1 mg of PCPP), while maintaining a consistency comparable to a gel (Figure 2B). In view of using this hydrogel as a drug delivery platform, we confirmed the capability of this hydrogel to load a range of alternative payloads (per 1 mg PCPP drug content of 405 μg of quisinostat, 370 μg of doxorubicin, or 46 μg of FITC-BSA, were loaded along with 10 mg AuNP each) (Figure 2C). The AuNP loaded hydrogel showed a red-shift of the surface plasmon resonance (Figure 2D), which is characteristic of the shortening of the intraparticles distances for AuNP,[36] and their dispersion in the hydrogel was confirmed by TEM (Figure 2E), elemental mapping, SEM and EDX analysis (Figure S5). FT-IR spectra showed peaks characteristic of both the PCPP (1550−1700 cm^{-1}, C=O stretching) and selenocystamine cross-linker (1250−1020 cm^{-1}, C−N stretching), while the peaks for C−Se and Se−Se bonds that are below 300 cm^{-1} are outside of our apparatus spectral range (Figure 2F).

The soft mechanical properties of Se-PCPP hydrogel permitted its easy injectability, were not affected by the loading with the payloads tested (Figure S6A and B), and showed both shear-thinning and elastic behaviors (storage modulus of 8 Pa and loss modulus of 1 Pa), as well as partial self-healing properties (Figure S6C and D) that are appealing for an easy administration with a syringe during craniotomy. Furthermore, AuNP produce strong contrast enhancement in CT, hence their loading in the Se-PCPP hydrogel made it opaque to radiation and trackable by CT for indirect monitoring of its degradation in a noninvasive manner and without a depth penetration limit (Figure S7).

3.5. Radiation Triggered Degradation and Payload Release from the Se-PCPP Hydrogel. Enhancing drug delivery as a response to radiation that has no depth penetration limit is appealing for personalized medicine and has the potential to synergize with radiotherapy. Of importance, the standard radiotherapy dose for GBM patients after surgical resection is over 66 Gy and can exceed 80 Gy in patients receiving radiation escalation.[37] Herein, administration of a single radiation dose of 60 Gy was preferred to compare with standard of care, and this radiation dose increased the release of AuNP by a factor of 3, confirming the radiation triggered degradation of Se-PCPP hydrogel (Figure 2G). On the other hand, irradiation with low radiation doses had a moderate effect (Figure S8A). Of note, the loading of the payloads we tested did not affect the AuNP release rate after irradiation (Figure S8B). Radiation triggered delivery proved also effective for other payloads (Figure S8C), with up to 93% of drug being released 7 days after treatment (Figure 2H). The slower delivery profile of FITC-BSA is likely due to its markedly higher molecular weight. The hydrogels' mechanical properties were unaffected by storage and 7 days of incubation

at 37 °C, while hydrogel irradiation by 60 Gy induced the partial loss of mechanical properties (Figure S8D).

More evidence of the radiation enhanced drug delivery was obtained in vitro by first irradiating the drug-loaded hydrogel with 60 Gy and incubating with cell medium for 24 h to allow the drug release. Then, this hydrogel supernate was used to treat U251 and NS039 cells. A decrease of cell viability of 73% was observed due to triggered drug release, while the effect was negligible without the trigger (Figure 2I). Since the above-mentioned conditions did not include cells' treatment with radiotherapy, in a second experiment, we compared the effect on cell viability of a combined treatment of radiotherapy to the cells and incubation with our X-ray (XR) degradable hydrogel. An 8 Gy radiotherapy dose was administered to the cells to allow an appreciable visualization of both effects in parallel rather than an intense cell killing effect due to high radiotherapy dose. After receiving 8 Gy radiotherapy, the cells were incubated with our X-ray (XR) degradable hydrogel, which had previously been exposed to either mock irradiation as control or 60 Gy radiation to trigger the drug release (Figure 2J). The combination of RT to the cells and XR triggered drug delivery showed a decrease of 22% and 25% of cell viability compared to the absence of RT on the cells or without the XR triggered drug release, respectively. In contrast, the non-degradable hydrogel did not show a significantly greater effect on cell viability after exposure to the X-ray trigger. Hence, this confirms the ability of the radiation degradable hydrogel at delivering a cytotoxic amount of drug in response to radiation trigger, and a synergy with cells exposure to RT. Of note, the drug-free Se-PCPP hydrogel showed high in vitro biocompatibility on a range of cancer and noncancer cells (Figure S9A), as did the degradation byproducts of the drug-free hydrogel (Figure S9B). This indicates that no toxicity arises in vitro from the degradation byproducts of the hydrogel.

Diselenium-containing molecules were suggested to be degradable after radiation mediated production of radical oxygen species (ROS).[38] Hence, to gain information on the mechanisms involved in the radiation triggered delivery that was observed herein, we investigated the effect of radiation on the Se-PCPP hydrogel in conditions preventing ROS formation, that is, in degassed medium or the presence of ROS scavengers. Both conditions that prevented ROS production also precluded the effects of radiation on hydrogel's degradation. This suggests an indirect degradation mechanism caused by radiation induced ROS production by radiolysis, and subsequent ROS induced Se−Se rupture causing hydrogel degradation (Figure S10A and B). More evidence of the necessity of the diselenium cross-linker to access radiation triggered delivery from the hydrogel was obtained using a control hydrogel termed C-PCPP that was cross-linked with the radiation insensitive hexamethylenediamine, and showed AuNP release profiles unaffected by radiation (Figure S10C and D). This provides evidence that supports the role of selenocystamine as a radiation degradable cross-linker.

3.6. High Therapeutic Efficiency and Prevention of Relapse Achieved by Combination of the Drug-Loaded Se-PCPP Hydrogel and Irradiation. The in vivo potential for Se-PCPP hydrogel at inhibiting GBM tumor growth by combination therapy (radiation triggered drug delivery and radiotherapy), was investigated on nude mice xenografted with human GBM tumors. The main treatment group of mice that received both injection of the hydrogel loaded with drug and radiation therapy (referred to as group H+drug+RT) was
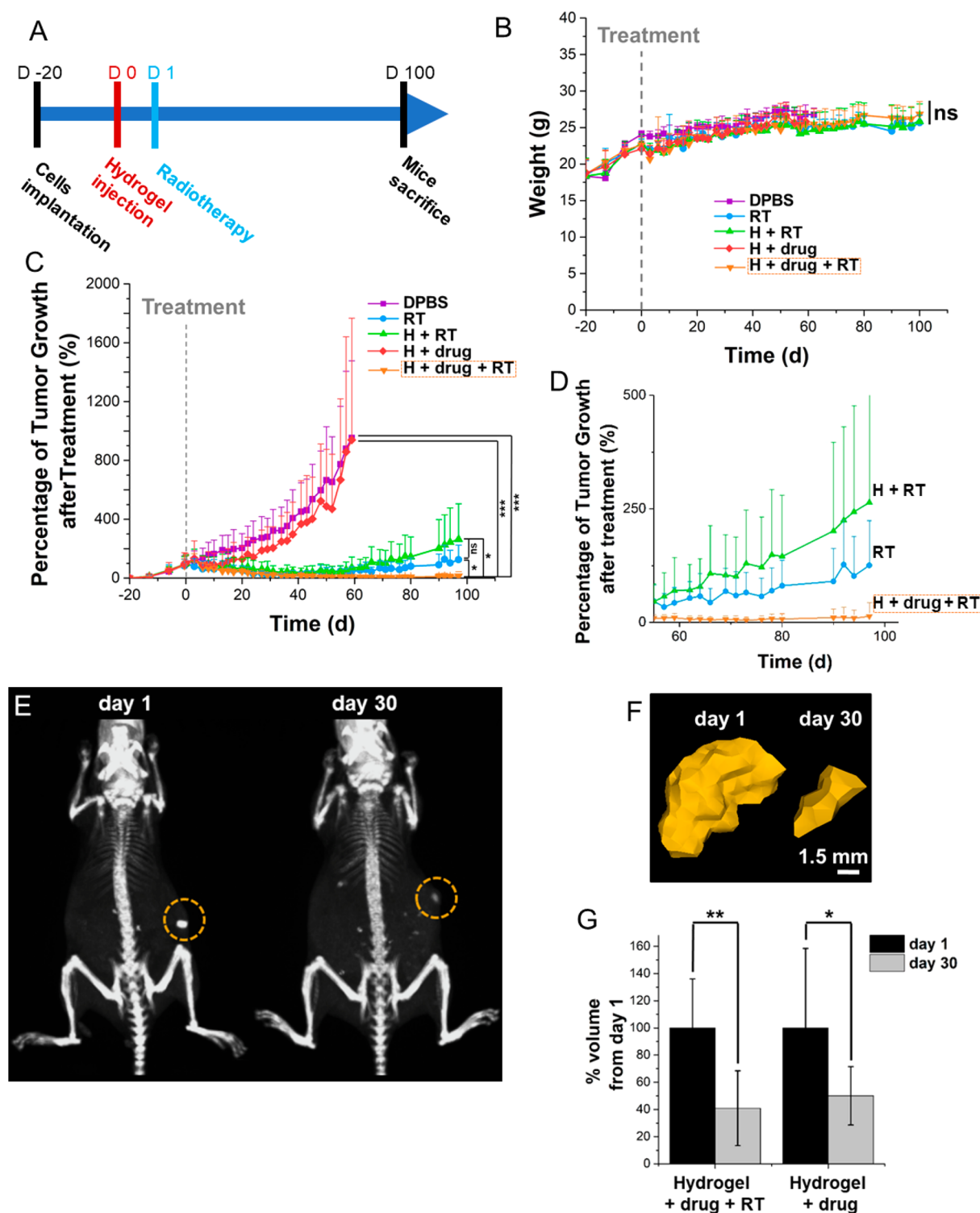
Figure 3. In vivo evaluation of the antitumoral effect of the quisinostat loaded Se-PCPP hydrogel and tolerability over 100 days, as well as in vivo hydrogel monitoring by CT. (A) Experimental design and evaluation of the (B) mouse weights and (C) tumor growth over 100 days. (D) Data shown in panel C with a focus on 55−100 days post treatment. (E) CT scans at 1 h and 30 days postinjection; the circles indicate the hydrogel. The windows level is 575 HU and the window width is 1250 HU. (F) 3D reconstructions of the hydrogel based on CT images. The AuNP loaded hydrogel was artificially colored in gold based on intensity thresholding using the same windows level and width as in A. (G) Quantification of the hydrogel degradation by comparing the volume change ($n = 6$).*, **, and *** indicate a difference at $p < 0.05$, 0.01, or 0.001, respectively, while ns indicates a nonsignificant difference.

compared to four control groups (vehicle labeled DPBS, radiotherapy labeled RT, hydrogel non-drug loaded followed by radiotherapy labeled H+RT and drug-loaded hydrogel labeled H+drug). The selected radiotherapy dose for in vivo investigation in this study was 10 Gy. This is a typical dose for preclinical testing of radiotherapy on mice,[39] which require the use of different radiation doses to humans. Treatments consisted of intratumoral injection of drug loaded or drug

free hydrogel or DPBS and local radiotherapy treatment of 10 or 0 Gy at 24 h postinjection (Figure 3A), as detailed in the supplementary file. Mice from H+drug+RT group (*orange*) showed no loss of weight or signs of adverse effects compared to control groups, suggesting the absence of apparent systemic toxicity and the high tolerability to Se-PCPP hydrogel and its components (Figure 3B).

A strong tumor growth inhibition was observed thanks to the combination of the drug loaded Se-PCPP hydrogel with radiation therapy (Figure 3C and D), leading to the complete response (CR) and absence of relapse of 67% of the cohort, which was statistically different to the control groups. In comparison, treatment with the drug loaded hydrogel in the absence of trigger showed no response, possibly due to the slow drug release kinetics occurring by passive elution. On the other hand, while both the radiotherapy alone and its combination with the drug-free hydrogel showed a partial response (PR) over the first 40 days, mice were found to relapse, leading to markedly larger tumors than the group H+drug+RT (Figure S11A and B). Overall, the cohort treated with drug loaded hydrogel combined with radiation demonstrated high levels of complete response, compared to all other groups.

3.7. Se-PCPP hydrogel degradation monitoring by CT. Imaging the injected hydrogel and monitoring its fate is of importance to gain insights into the delivery kinetic of payloads, and to confirm its biodegradability. To address the long-term monitoring of the radiopaque Se-PCPP hydrogel, we used CT imaging which allows both the tracking of the AuNP payload in the hydrogel and its quantification, and fits with the clinical regimen. The dense concentration of AuNP in the compact hydrogel formed at the intratumoral injection site granted its visualization and delineation from the surrounding tumor tissues (Figure 3E), and could be reconstructed as a 3D image using a region growing method based on contrast enhancement thresholds (Figure 3F). Moreover, the volume of the hydrogels quantified by CT was found to significantly decrease to 41% (10 Gy) and 50% (0 Gy) at 30 days postinjection (Figure 3G). Hence, hydrogel monitoring using CT confirmed the successful in vivo biodegradability of the Se-PCPP hydrogel over time.

3.8. Biodistribution of Released AuNP and Pathology Investigation. Furthermore, sub-5 nm AuNP were chosen for loading in the Se-PCPP hydrogel owing to their excretion profile through kidneys and urine that limits body retention.[40,41] Major organs in group H+drug+RT showed minimal AuNP retention (cumulated gold content in major organs of 12% of the ID/g) (Figure S11C). On the other hand, the highest concentration of gold, that is, 5% ID/g, was found in the tumor and corresponds to the remaining hydrogel.

The in vivo tolerability of the Se-PCPP hydrogel and the negligible body accumulation of AuNP were confirmed by histopathological examination of major organs. The H+drug+RT group showed neither obvious histopathological lesions nor structural differences compared to the control group "DPBS", confirming the high tolerability of the quisinostat-loaded hydrogel by mice (Figure S12). These preliminary findings support the high tolerability over long-term of quisinostat when loaded in the Se-PCPP hydrogel, which contrasts with the occurrence of side effects when quisinostat is administered systematically, and indicate its in vivo safety.

4. DISCUSSION

Altogether, our results highlight this novel radiation responsive Se-PCPP hydrogel as an effective drug delivery platform for the treatment of GBM. The acute tumor growth inhibition observed using this combination treatment resulted in a CR rate of 67%, which may be due to the longer drug retention time in the GBM area compared to systemic administration, as already assessed by others.[42−47] The absence of visible side effects or histopathological lesions after Se-PCPP hydrogel administration suggested the favorable tolerability of the hydrogel and its components, and correlated with other polyphosphazene-based hydrogels,[46,47] although more extensive safety-related investigation will be needed in the future.

Moreover, AuNP loading in the hydrogel enabled the monitoring of its degradability and in vivo behavior by quantification of the volume and HU values using CT, as already shown by Lei et al.[48] Alternatively, hydrogel design could be adapted for in vivo tracking by other medical imaging techniques, including fluorescence using tagged polymers[49] or aggregation induced emission (AIE),[50] although shorter residence times were observed with such formulations compared to our Se-PCPP hydrogel.[51] Hence, our hydrogel compares favorably with other drug delivery hydrogels for the treatment of GBM.[38,52,53]

The present study stands as a proof-of-concept for the opportunities offered by selenocystamine cross-linked PCPP hydrogel for the local treatment of deep lying cancers by radiation triggered drug delivery. The radiation trigger selected herein is advantageous compared to other external stimuli, such as light or ultrasound radiation, that suffer depth penetration limits, that hinders their use for deep tumors such as GBM,[54−57] although the reduction of radiation dose required, ideally below the standard radiation dose of 60 Gy used in humans, remains a challenge. The sensitivity of diselenium to redox changes[58,59] and radiation triggered degradation has already proved promising by others,[60,61] and progress toward enhancing the sensitivity of our diselenium cross-linker and Se-PCPP hydrogel toward lower doses of radiation may be beneficial, for example by replacing selenium with tellurium.[62] Alternatively, FLASH radiotherapy (FLASH-RT), where high doses of radiation are delivered at an ultrahigh dose rate to enhance the therapeutic efficacy while minimizing the toxicity to the surrounding tissues[63] may be applicable to our current platform.[64−66]

Overall, the easy production of this hydrogel, its adaptability and moderate stiffness are beneficial for a standardized and convenient syringe administration. Moreover, the high tolerability of both the hydrogel and its degradation byproducts that was assessed in vitro and in vivo, make this novel Se-PCPP hydrogel formulation a promising platform with advantageous translational abilities for patient care in the treatment of GBM. Accordingly, longer-term studies of the in vivo degradation and biocompatibility of the hydrogel will be needed to fully understand its potential role in therapies. Its adaptability to deliver payloads ranging in nature from small, hydrophobic molecules, to much larger, hydrophilic proteins or AuNP, foreshadows its use for a broader range of drugs in the management of cancer or other diseases such as diabetes. Likewise, loading of other contrast agents in Se-PCPP hydrogel would be of interest to access a broader range of imaging modalities.[52,67]

5. CONCLUSION

In this study, we introduce a promising treatment for GBM using an injectable Se-PCPP hydrogel, capable of drug release upon a radiation trigger. It allowed the delivery of an effective anti-GBM drug, quisinostat, and showed no signs of systemic toxicity. The diselenium cross-linker enabled the stimulus-responsive degradability by radiation, and significantly enhanced the in vitro drug release profile after radiation triggered degradation. Moreover, the in vivo results confirmed the strong tumor inhibition capability of this drug loaded hydrogel in combination with radiotherapy, showing an elevated rate of CR, and preventing long-term relapse which remains a challenge with current therapeutic options. Furthermore, monitoring the long residence time and biodegradability of the hydrogel by CT was possible because of the radiopaque AuNP loaded in the hydrogel. Finally, the long-term tolerability of both the Se-PCPP hydrogel and its degradation byproducts was evidenced both in vitro and in vivo by the absence of either visible side effects on the animal health or abnormalities on the organ structure. Overall, this hydrogel presents beneficial features for local chemotherapy administration and radiotherapy combination therapy of GBM, without inducing visible side effects, and its adaptability allows for loading of high payloads of drugs and nanoparticles, thus foreshadowing its potential as an "on-demand" drug delivery biomaterial for personalized medicine.

■ ASSOCIATED CONTENT

ⓈⒾ Supporting Information

The Supporting Information is available free of charge at https://pubs.acs.org/doi/10.1021/acsbiomaterials.1c00385.

> Materials; cell-based high-throughput death receptor screen; Western blot analysis; compound dilution studies and cell viability; sphere formation assay; primary brain tumor specimens; brain tumor organoids, compound incubation, and viability; immunofluorescence; orthotopic tumor implantation and treatment with quisinostat; gold nanoparticle synthesis; Se-PCPP hydrogel formulation: cargo-loaded Se-PCPP hydrogel, C-PCPP hydrogel; hydrogel characterization, UV−vis spectroscopy, transmission electron microscopy (TEM), scanning electron microscopy (SEM), Fourier transform infrared (FT-IR), inductively coupled plasma optical emission spectroscopy (ICP-OES), vial inversion, rheology, and injection force; X-ray irradiation; hydrogels degradation and cargo release experiments; cell culture; computed tomography (CT) phantom imaging; in vivo rodent model of xenografted GBM, intratumoral injection, in vivo CT, and in vivo radiotherapy; survival analysis of xenografted mice; organs harvesting and ex vivo investigation; and statistical analysis (PDF)

■ AUTHOR INFORMATION

Corresponding Authors

Mathilde Bouché − *Department of Radiology, University of Pennsylvania, Philadelphia, Pennsylvania 19104, United States;* ⓞ orcid.org/0000-0003-2707-1290; Email: Mathilde.Bouche9@gmail.com

David P. Cormode − *Department of Radiology, University of Pennsylvania, Philadelphia, Pennsylvania 19104, United States; Department of Bioengineering, University of Pennsylvania, Philadelphia, Pennsylvania 19104, United States;* ⓞ orcid.org/0000-0002-8391-9500; Phone: 215-615-4656; Email: David.Cormode@pennmedicine.upenn.edu; Fax: 240-368-8096

Authors

Yuxi C. Dong − *Department of Radiology, University of Pennsylvania, Philadelphia, Pennsylvania 19104, United States; Department of Bioengineering, University of Pennsylvania, Philadelphia, Pennsylvania 19104, United States;* ⓞ orcid.org/0000-0001-7739-3795

Saad Sheikh − *Department of Radiation Oncology, University of Pennsylvania, Philadelphia, Pennsylvania 19104, United States*

Kimberly Taing − *Department of Radiology, University of Pennsylvania, Philadelphia, Pennsylvania 19104, United States*

Deeksha Saxena − *Department of Radiation Oncology, University of Pennsylvania, Philadelphia, Pennsylvania 19104, United States*

Jessica C. Hsu − *Department of Radiology, University of Pennsylvania, Philadelphia, Pennsylvania 19104, United States; Department of Bioengineering, University of Pennsylvania, Philadelphia, Pennsylvania 19104, United States*

Minna H. Chen − *Department of Bioengineering, University of Pennsylvania, Philadelphia, Pennsylvania 19104, United States*

Ryan D. Salinas − *Department of Neurosurgery, University of Pennsylvania, Philadelphia, Pennsylvania 19104, United States*

Hongjun Song − *Department of Neuroscience, University of Pennsylvania, Philadelphia, Pennsylvania 19104, United States*

Jason A. Burdick − *Department of Bioengineering, University of Pennsylvania, Philadelphia, Pennsylvania 19104, United States;* ⓞ orcid.org/0000-0002-2006-332X

Jay Dorsey − *Department of Radiation Oncology, University of Pennsylvania, Philadelphia, Pennsylvania 19104, United States*

Complete contact information is available at:
https://pubs.acs.org/10.1021/acsbiomaterials.1c00385

Notes

The authors declare the following competing financial interest(s): M. B., D. P. C., S. S., and J. D. are named on a patent application focusing on radiation responsive hydrogels.

■ REFERENCES

(1) Alexander, B. M.; Cloughesy, T. F. Adult Glioblastoma. *J. Clin. Oncol.* **2017**, *35* (21), 2402.

(2) Shergalis, A.; Bankhead, A.; Luesakul, U.; Muangsin, N.; Neamati, N. Current challenges and opportunities in treating glioblastoma. *Pharmacol. Rev.* **2018**, *70* (3), 412.

(3) Delgado-Lopez, P. D.; Corrales-Garcia, E. M. Survival in glioblastoma: a review on the impact of treatment modalities. *Clin. Transl. Oncol.* **2016**, *18* (11), 1062.

(4) Sanai, N.; Berger, M. S. Surgical oncology for gliomas: the state of the art. *Nat. Rev. Clin. Oncol.* **2018**, *15* (2), 112.

(5) Mann, J.; Ramakrishna, R.; Magge, R.; Wernicke, A. G. Advances in radiotherapy for glioblastoma. *Front. Neurol.* **2018**, *8*, 748.

(6) Singh, S. K.; Clarke, I. D.; Terasaki, M.; Bonn, V. E.; Hakins, C.; Squire, J.; Dirks, P. B. Identification of a cancer stem cell in human brain tumors. *Cancer Res.* **2003**, *63* (18), 5821.

(7) Galli, R.; Binda, E.; Orfanelli, U.; Cipelletti, B.; Gritti, A.; De Vitis, S.; Fiocco, R.; Foroni, C.; Dimeco, F.; Vescovi, A. Isolation and characterization of tumorigenic, stem-like neural precursors from human glioblastoma. *Cancer Res.* **2004**, *64* (19), 7011.

(8) Bao, S.; Wu, Q.; McLendon, R. E.; Hao, Y.; Shi, Q.; Hjelmeland, A. B.; Dewhirst, M. W.; Bigner, D. D.; Rich, J. N. Glioma stem cells promote radioresistance by preferential activation of the DNA damage response. *Nature* **2006**, *444* (7120), 756.

(9) Liu, G.; Yuan, X.; Zeng, Z.; Tunici, P.; Ng, H.; Abdulkadir, I. R.; Lu, L.; Irvin, D.; Black, K. L.; Yu, J. S. Analysis of gene expression and chemoresistance of CD133+ cancer stem cells in glioblastoma. *Mol. Cancer* **2006**, *5*, 67.

(10) Bartek, J.; Ng, K.; Bartek, J.; Fischer, W.; Carter, B.; Chen, C. C. Key concepts in glioblastoma therapy. *J. Neurol., Neurosurg. Psychiatry* **2012**, *83*, 753.

(11) Zhou, B. B.; Zhang, H.; Damelin, M.; Geles, K. G.; Grindley, J. C.; Dirks, P. B. Tumour-initiating cells: challenges and opportunities for anticancer drug discovery. *Nat. Rev. Drug Discovery* **2009**, *8* (10), 806.

(12) Walczak, H.; Miller, R. E.; Ariail, K.; Gliniak, B.; Griffith, T. S.; Kubin, M.; Chin, W.; Jones, J.; Woodward, A.; Le, T.; Smith, C.; Smolak, P.; Goodwin, R. G.; Rauch, C. T.; Schuh, J. C.; Lynch, D. H. Tumoricidal activity of tumor necrosis factor-related apoptosis-inducing ligand in vivo. *Nat. Med.* **1999**, *5* (2), 157.

(13) Ganipineni, L. P.; Danhier, F.; Préat, V. Drug delivery challenges and future of chemotherapeutic nanomedicine for glioblastoma treatment. *J. Controlled Release* **2018**, *281*, 42.

(14) Ghosh, D.; Nandi, S.; Bhattacharjee, S. Combination therapy to checkmate Glioblastoma: clinical challenges and advances. *Clin. Transl. Med.* **2018**, *7* (1), 33.

(15) Wolinsky, J. B.; Colson, Y. L.; Grinstaff, M. W. Local drug delivery strategies for cancer treatment: gels, nanoparticles, polymeric films, rods, and wafers. *J. Controlled Release* **2012**, *159* (1), 14.

(16) Brem, H; Piantadosi, S; Burger, P.C; Walker, M; Selker, R; Vick, N.A; Black, K; Sisti, M; Brem, S; Mohr, G; Muller, P; Morawetz, R; Schold, S.C Placebo-controlled trial of safety and efficacy of intraoperative controlled delivery by biodegradable polymers of chemotherapy for recurrent gliomas. The Polymer-brain Tumor Treatment Group. *Lancet* **1995**, *345* (8956), 1008.

(17) Rosenblum, M. K.; Delattre, J. Y.; Walker, R. W.; Shapiro, W. R. Fatal necrotizing encephalopathy complicating treatment of malignant gliomas with intra-arterial BCNU and irradiation: a pathological study. *J. Neuro-Oncol.* **1989**, *7*, 269.

(18) Pereira, D. Y.; Yip, A. T.; Lee, B. S.; Kamei, D. T. Modeling mass transfer from carmustine-loaded polymeric implants for malignant gliomas. *J. Lab. Autom.* **2014**, *19* (1), 19.

(19) Tabet, A.; Jensen, M. P.; Parkins, C. C.; Patil, P. G.; Watts, C.; Scherman, O. A. Designing next-generation local drug delivery vehicles for glioblastoma adjuvant chemotherapy: lessons from the clinic. *Adv. Healthcare Mater.* **2019**, *8* (3), 1801391.

(20) Sheikh, S.; Saxena, D.; Tian, X.; Amirshaghaghi, A.; Tsourkas, A.; Brem, S.; Dorsey, J. F. An integrated stress response agent that modulates DR5-dependent TRAIL synergy reduces patient-derived glioma stem cell viability. *Mol. Cancer Res.* **2019**, *17* (5), 1102.

(21) Ullah, F.; Othman, M. B. H.; Javed, F.; Ahmad, Z.; Akil, H. M. Classification, processing and application of hydrogels: A review. *Mater. Sci. Eng., C* **2015**, *57*, 414.

(22) Koetting, M. C.; Peters, J. T.; Steichen, S. D.; Peppas, N. A. Stimulus-responsive hydrogels: Theory, modern advances, and applications. *Mater. Sci. Eng., R* **2015**, *93*, 1.

(23) Basso, J.; Miranda, A.; Nunes, S.; Cova, T.; Sousa, J.; Vitorino, C.; Pais, A. Hydrogel-based drug delivery nanosystems for the treatment of brain tumors. *Gels* **2018**, *4* (3), 62.

(24) Bianco, J.; Bastiancich, C.; Jankovski, A.; des Rieux, A.; Préat, V.; Danhier, F. On glioblastoma and the search for a cure: where do we stand? *Cell. Mol. Life Sci.* **2017**, *74*, 2451.

(25) Xue, K.; Wang, X.; Yong, P. W.; Young, D. J.; Wu, Y.-L.; Li, Z.; Loh, X. J. Hydrogels as emerging materials for translational biomedicine. *Adv. Therapeutics* **2019**, *2* (1), 1800088.

(26) Liu, J.; Zhang, Y.; Li, Q.; Feng, Z.; Huang, P.; Wang, W.; Liu, J. Development of injectable thermosensitive polypeptide hydrogel as facile radioisotope and radiosensitizer hotspot for synergistic brachytherapy. *Acta Biomater.* **2020**, *114*, 133.

(27) Wang, W.; Song, H.; Zhang, J.; Li, P.; Li, C.; Wang, C.; Kong, D.; Zhao, Q. An injectable, thermosensitive and multicompartment hydrogel for simultaneous encapsulation and independent release of a drug cocktail as an effective combination therapy platform. *J. Controlled Release* **2015**, *203*, 57.

(28) Andrianov, A. K.; Marin, A.; Chen, J. Synthesis, properties, and biological activity of poly[di(sodium carboxylatoethylphenoxy)-phosphazene]. *Biomacromolecules* **2006**, *7* (1), 394.

(29) Cheheltani, R.; Ezzibdeh, R. M.; Chhour, P.; Pulaparthi, K.; Kim, J.; Jurcova, M.; Hsu, J. C.; Blundell, C.; Litt, H. I.; Ferrari, V. A.; Allcock, H. R.; Sehgal, C. M.; Cormode, D. P. Tunable, biodegradable gold nanoparticles as contrast agents for computed tomography and photoacoustic imaging. *Biomaterials* **2016**, *102*, 87.

(30) Hajfathalian, M.; Bouché, M.; Cormode, D. P. Polyphospha-zene-based nanoparticles as contrast agents, Chapter. *ACS Symp. Ser.* **2018**, *1298*, 77.

(31) Kim, J.; Silva, A. B.; Hsu, J. C.; Maidment, P. S. N.; Shapira, N.; Noël, P. B.; Cormode, D. P. Radioprotective garment-inspired biodegradable polymetal nanoparticles for enhanced CT contrast production. *Chem. Mater.* **2020**, *32* (1), 381.

(32) Andrianov, A. K.; Marin, A.; Fuerst, T. R. Molecular-level interactions of polyphosphazene immunoadjuvants and their potential role in antigen presentation and cell stimulation. *Biomacromolecules* **2016**, *17* (11), 3732.

(33) Mieszawska, A. J.; Mulder, W. J. M.; Fayad, Z. A.; Cormode, D. P. Multifunctional gold nanoparticles for diagnosis and therapy of disease. *Mol. Pharmaceutics* **2013**, *10* (3), 831.

(34) Chhour, P.; Gallo, N.; Cheheltani, R.; Williams, D.; Al-Zaki, A.; Paik, T.; Nichol, J. L.; Tian, Z.; Naha, P. C.; Witschey, W. R.; Allcock, H. R.; Murray, C. B.; Tsourkas, A.; Cormode, D. P. Nanodisco balls: control over surface versus core loading of diagnostically active nanocrystals into polymer nanoparticles. *ACS Nano* **2014**, *8*, 9143.

(35) Jacob, F.; Salinas, R. D.; Zhang, D. Y.; Nguyen, P. T.T.; Schnoll, J. G.; Wong, S. Z. H.; Thokala, R.; Sheikh, S.; Saxena, D.; Prokop, S.; Liu, D.-a.; Qian, X.; Petrov, D.; Lucas, T.; Chen, H. I.;

Dorsey, J. F.; Christian, K. M.; Binder, Z. A.; Nasrallah, M.; Brem, S.; O'Rourke, D. M.; Ming, G.-l.; Song, H. A Patient-derived glioblastoma organoid model and biobank recapitulates inter- and intra-tumoral heterogeneity. *Cell* **2020**, *180* (1), 188.

(36) Bouché, M.; Pühringer, M.; Iturmendi, A.; Amirshaghaghi, A.; Tsourkas, A.; Teasdale, I.; Cormode, D. P. Activatable hybrid polyphosphazene-AuNP nanoprobe for ROS detection by bimodal PA/CT imaging. *ACS Appl. Mater. Interfaces* **2019**, *11* (32), 28648.

(37) Wegner, R. E.; Abel, S.; Horne, Z. D.; Hasan, S.; Verma, V.; Ranjan, T.; Williamson, R. W.; Karlovits, S. M. National trends in radiation dose escalation for glioblastoma. *Radiat. Oncol. J.* **2019**, *37* (1), 13.

(38) Xu, H.; Cao, W.; Zhang, X. Selenium-containing polymers: promising biomaterials for controlled release and enzyme mimics. *Acc. Chem. Res.* **2013**, *46* (7), 1647.

(39) Sun, L. Q.; Vogel, C. A.; Mirimanoff, R. O.; Coucke, P.; Slosman, D. O.; Mach, J. P.; Buchegger, F. Timing effects of combined radioimmunotherapy and radiotherapy on a human solid tumor in nude mice. *Cancer Res.* **1997**, *57* (7), 1312.

(40) Hirn, S.; Semmler-Behnke, M.; Schleh, C.; Wenk, A.; Lipka, J.; Schäffler, M.; Takenaka, S.; Möller, W.; Schmid, G.; Simon, U.; Kreyling, W. G. Particle size-dependent and surface charge-dependent biodistribution of gold nanoparticles after intravenous administration. *Eur. J. Pharm. Biopharm.* **2011**, *77* (3), 407.

(41) Poon, W.; Zhang, Y.-N.; Ouyang, B.; Kingston, B. R.; Wu, J. L. Y.; Wilhelm, S.; Chan, W. C. W. Elimination pathways of nanoparticles. *ACS Nano* **2019**, *13* (5), 5785.

(42) Bastiancich, C.; Bianco, J.; Vanvarenberg, K.; Ucakar, B.; Joudiou, N.; Gallez, B.; Bastiat, G.; Lagarce, F.; Préat, V.; Danhier, F. Injectable nanomedicine hydrogel for local chemotherapy of glioblastoma after surgical resection. *J. Controlled Release* **2017**, *264*, 45.

(43) Joh, D. Y.; Sun, L.; Stangl, M.; Al-Zaki, A.; Murty, S.; Santoiemma, P. P.; Davis, J. J.; Baumann, B. C.; Alonso-Basanta, M.; Bhang, D.; Kao, G. D.; Tsourkas, A.; Dorsey, J. F. Selective targeting of brain tumors with gold nanoparticle-induced radiosensitization. *PLoS One* **2013**, *8* (4), No. e62425.

(44) Sun, L.; Joh, D. Y.; Al-Zaki, A.; Stangl, M.; Murty, S.; Davis, J. J.; Baumann, B. C.; Alonso-Basanta, M.; Kao, G. D.; Tsourkas, A.; Dorsey, J. F. Theranostic application of mixed gold and superparamagnetic iron oxide nanoparticle micelles in glioblastoma multiforme. *J. Biomed. Nanotechnol.* **2016**, *12* (2), 347.

(45) Zhang, Z. Q.; Song, S. C. Thermosensitive/superparamagnetic iron oxide nanoparticle-loaded nanocapsule hydrogels for multiple cancer hyperthermia. *Biomaterials* **2016**, *106*, 13.

(46) Seo, B.-B.; Chang, H.-I.; Choi, H.; Koh, J.-T.; Yun, K.-D.; Lee, J.-Y.; Song, S.-C. New approach for vertical bone regeneration using in situ gelling and sustained BMP-2 releasing poly(phosphazene) hydrogel system on peri-implant site with critical defect in a canine model. *J. Biomed. Mater. Res., Part B* **2018**, *106* (2), 751.

(47) Song, S.-C.; Kim, Y.-M. Poly(organophosphazene) containing degradation controllable ionic group, preparation method thereof and use thereof. US 2014031289-A1, 2012.

(48) Lei, K.; Chen, Y.; Wang, J.; Peng, X.; Yu, L.; Ding, J. Non-invasive monitoring of in vivo degradation of a radiopaque thermoreversible hydrogel and its efficacy in preventing post-operative adhesions. *Acta Biomater.* **2017**, *55*, 396.

(49) Artzi, N.; Oliva, N.; Puron, C.; Shitreet, S.; Artzi, S.; bon Ramos, A.; Groothuis, A.; Sahagian, G.; Edelman, E. R. In vivo and in vitro tracking of erosion in biodegradable materials using non-invasive fluorescence imaging. *Nat. Mater.* **2011**, *10* (9), 890.

(50) Liow, S. S.; Dou, Q.; Kai, D.; Li, Z.; Sugiarto, S.; Yu, C. Y.; Kwok, R. T.; Chen, X.; Wu, Y. L.; Ong, S. T.; Kizhakeyil, A.; Verma, N. K.; Tang, B. Z.; Loh, X. J. Long-term real-time in vivo drug release monitoring with AIE thermogelling polymer. *Small* **2017**, *13* (7), 1603404.

(51) Qin, L.; Cao, J.; Shao, K.; Tong, F.; Yang, Z.; Lei, T.; Wang, Y.; Hu, C.; Umeshappa, C. S.; Gao, H.; Peppas, N. A. A tumor-to-lymph procedure navigated versatile gel system for combinatorial therapy against tumor recurrence and metastasis. *Sci. Adv.* **2020**, *6* (36), No. eabb3116.

(52) Kim, J. I.; Kim, B.; Chun, C.; Lee, S. H.; Song, S. C. MRI-monitored long-term therapeutic hydrogel system for brain tumors without surgical resection. *Biomaterials* **2012**, *33* (19), 4836.

(53) Zhao, M.; Bozzato, E.; Joudiou, N.; Ghiassinejad, S.; Danhier, F.; Gallez, B.; Préat, V. Codelivery of paclitaxel and Temozolomide through a photopolymerizable hydrogel prevents glioblastoma recurrence after surgical resection. *J. Controlled Release* **2019**, *309*, 72.

(54) Lobez, J. M.; Swager, T. M. Radiation detection: resistivity responses in functional poly(olefin sulfone)/carbon nanotube composites. *Angew. Chem., Int. Ed.* **2010**, *49* (1), 95.

(55) Brown, J. R.; O'Donnell, J. H. γ Radiolysis of poly(butene-1 sulfone) and poly(hexene-1 sulfone). *Macromolecules* **1972**, *5*, 109.

(56) Harada, S.; Ehara, S.; Ishii, K.; Yamazaki, H.; Matsuyama, S.; Kamiya, T.; Sakai, T.; Arakawa, K.; Sato, T.; Oikawa, S. Improvement of radiosensitive liquid-core microcapsules by Yttrium polymerization. *Nucl. Instrum. Methods Phys. Res., Sect. B* **2007**, *260* (1), 164.

(57) Lamberts, H. B.; Alexander, P. Post-irradiation changes in solutions of hyaluronic acid exposed to X-rays. *Biochim. Biophys. Acta, Spec. Sect. Biophys. Subj.* **1964**, *88* (3), 642.

(58) Xia, J.; Li, T.; Lu, C.; Xu, H. P. Selenium-containing polymers: perspectives toward diverse applications in both adaptive and biomedical materials. *Macromolecules* **2018**, *51*, 7435.

(59) Fan, Z.; Xu, H. P. Interface design for high energy density polymer nanocomposites. *Polym. Rev.* **2020**, *60* (1), 114.

(60) Ma, N.; Xu, H.; An, L.; Li, J.; Sun, Z.; Zhang, X. Radiation-sensitive diselenide block co-polymer micellar aggregates: toward the combination of radiotherapy and chemotherapy. *Langmuir* **2011**, *27*, 5874.

(61) Cao, W.; Zhang, X.; Miao, X.; Yang, Z.; Xu, H. γ-Ray-responsive supramolecular hydrogel based on a diselenide-containing polymer and a peptide. *Angew. Chem., Int. Ed.* **2013**, *52*, 6233.

(62) Fan, F. Q.; Gao, S. Q.; Ji, S. B.; Fu, Y.; Zhang, P. P.; Xu, H. P. Gamma radiation-responsive side-chain tellurium-containing polymer for cancer therapy. *Mater. Chem. Front.* **2018**, *2* (11), 2109.

(63) Bourhis, J.; Montay-Gruel, P.; Gonçalves Jorge, P.; Bailat, C.; Petit, B.; Ollivier, J.; Jeanneret-Sozzi, W.; Ozsahin, M.; Bochud, F.; Moeckli, R.; Germond, J.-F.; Vozenin, M.-C. Treatment of a first patient with FLASH-radiotherapy. *Radiother. Oncol.* **2019**, *139*, 11.

(64) Symonds, P.; Jones, G. D. D. FLASH radiotherapy: the next technological advance in radiation therapy? *Clin. Oncol.* **2019**, *31* (7), 405.

(65) Spitz, D. R.; Buettner, G. R.; Petronek, M. S.; St-Aubin, J. J.; Flynn, R. T.; Waldron, T. J.; Limoli, C. L. An integrated physico-chemical approach for explaining the differential impact of FLASH versus conventional dose rate irradiation on cancer and normal tissue responses. *Radiother. Oncol.* **2019**, *139*, 23.

(66) Simmons, D. A.; Lartey, F. M.; Schüler, E.; Rafat, M.; King, G.; Kim, A.; Ko, R.; Semaan, S.; Gonzalez, S.; Jenkins, M.; Pradhan, P.; Shih, Z.; Wang, J.; von Eyben, R.; Graves, E. E.; Maxim, P. G.; Longo, F. M.; Loo, B. W. Jr. Reduced cognitive deficits after FLASH irradiation of whole mouse brain are associated with less hippocampal dendritic spine loss and neuroinflammation. *Radiother. Oncol.* **2019**, *139*, 4.

(67) Kim, J. I.; Lee, B. S.; Chun, C.; Cho, J. K.; Kim, S. Y.; Song, S. C. Hypoxia-mimicking mesoporous bioactive glass scaffolds with controllable cobalt ion release for bone tissue engineering. *Biomaterials* **2012**, *33* (7), 2251.